Optically Transparent FTO-Free Cathode for Dye-Sensitized Solar Cells

Ladislav Kavan,*[†,‡] Paul Liska,[†] Shaik M. Zakeeruddin,[†] and Michael Grätzel[†]

[†]Laboratory of Photonics and Interfaces, Institute of Chemical Sciences and Engineering, Swiss Federal Institute of Technology, CH-1015 Lausanne, Switzerland

[‡]J. Heyrovský Institute of Physical Chemistry, v.v.i., Academy of Sciences of the Czech Republic, Dolejškova 3, CZ-18223 Prague 8, Czech Republic

S Supporting Information

ABSTRACT: The woven fabric containing electrochemically platinized tungsten wire is an affordable flexible cathode for liquid-junction dye-sensitized solar cells with the I_3^-/I^- redox mediator and electrolyte solution consisting of ionic liquids and propionitrile. The fabric-based electrode outperforms the thermally platinized FTO in serial ohmic resistance and charge-transfer resistance for triiodide reduction, and it offers comparable or better optical transparency in the visible and particularly in the near-IR spectral region. The electrode exhibits good stability during electrochemical loading and storage at open circuit. The dye-sensitized solar cells with a C101-sensitized titania photoanode and either Pt–W/PEN or Pt–FTO cathodes show a comparable performance.
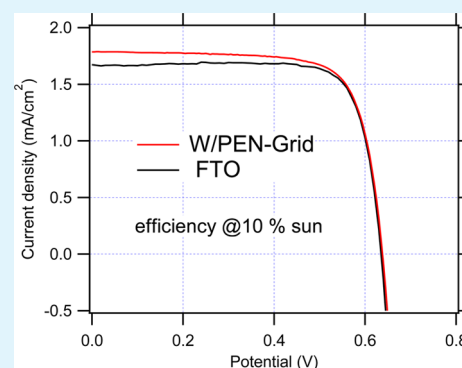
KEYWORDS: dye-sensitized solar cell, electrochemical impedance spectroscopy, tungsten electrode, woven fabric

1. INTRODUCTION

The dye-sensitized solar cell (DSC), also called the Grätzel cell, is an alternative to Si-based photovoltaics, offering comparable efficiency at lower cost and easier fabrication.[1–3] Recently, this concept has developed into the so-called perovskite solar cells, exhibiting remarkable performance with the certified solar to electric power conversion of 17.9%.[4,5] Traditional liquid-junction DSCs employ the sensitized TiO_2 photoanode supported by an F-doped SnO_2 (FTO) glass and platinized FTO glass as the cathode. The cost of FTO glass is estimated to be about 20–60% of the total cost of the practical DSC-module.[6–9] Hence, there is a strong motivation to replace FTO with cheaper materials. These alternatives should match FTO in the electrical conductivity (typically 10 Ω/sq) and in the optical transmittance for visible light (typically 80% near the peak of solar spectrum). Although the latter is not required for the proper function of DSCs, it is beneficial for certain applications such as in windows and roof panels.

The replacement of FTO by metallic meshes has been attempted, particularly for the TiO_2 photoanode using materials like Ti,[8,10,11] stainless steel,[6,11–13] or TiO_2-coated stainless steel;[7,13,14] in the last case, the titania coating improved the stability of steel against oxidation. Huang et al.[15] reported a DSC cathode fabricated from Cu–Ni mesh filled with conducting polymers and carbon black. Highly active cathode from stainless-steel-supported carbon black was developed by Murakami and Grätzel.[16] Carbon cloth,[17] graphene ribbons,[18] carbon nanosheets,[19] and carbon modified by Cu_2ZnSnS_4

nanodots[9] were tested recently as DSC cathodes, too. However, all these electrodes were, presumably opaque optically.

A transparent DSC cathode made from platinized Ti-mesh was reported by He et al.[11] However, their device exhibited poor fill factor (FF) ascribed to long diffusion paths across the openings of the grid. Recently, Bao et al.[20] improved the Ti-mesh counterelectrode by electrochemical oxidation toward TiO_2 nanotubes, which served as support for the Pt catalyst. Their DSC provided 6.3% solar conversion efficiency, which was close to that of a control device with a platinized FTO (Pt–FTO) cathode (6.4%). The use of platinized stainless steel mesh for DSC cathodes was reviewed by Toivola et al.[21] Interestingly, the deposition of platinum by thermal decomposition of H_2PtCl_6 (which is the standard protocol for FTO) did not work well on stainless steel, but sputtered Pt on steel was sufficiently active catalytically. FTO-free cathodes from platinum nanofiber webs[22] and nonwoven graphite fiber films[23] were reported, too.

There have been several attempts to fabricate DSCs by using fabric-based electrodes. Recently, Xu et al.[24] coated a common cotton textile fabric by Ni and polypyrrole and used it as a cathode in DSC. Although the electrocatalytic activity was good, the performance of their device was about half of that of control cell with a Pt–FTO cathode. Yun et al.[25] fabricated a

5.8% efficient DSC by sewing electrode wires on cloth; the electrodes consisted of stainless steel, Ti, and glass fibers.[25]

Hany et al.[26−28] applied transparent conductive woven fabric for organic photovoltaic cell with a poly(3-hexylthiophene) light harvester. They used either a pure polyimide fabric coated by poly(3,4-ethylenedioxythiophene):polystyrene sulfonic acid (PEDOT:PSS)[28] or a composite fabric woven from molybdenum wires and polyimide fibers functioning as warp and weft, respectively.[26,28] The sheet resistivity was from ≈1 to 9 Ω/sq (varying with metal/polymer ratio), which is outperforming that of most conductive glasses.[26−28] To the best of our knowledge, this kind of fabric was not yet tested as the electrode material in DSCs. Here, we report on successful replacement of Pt−FTO cathode in a classical I-mediated, liquid-junction DSC by platinized-tungsten/PEN fabric (PEN = poly(ethylene 2,6-naphthalate)).

2. RESULTS AND DISCUSSION

Our preliminary experiments focused on eutectic melt of ionic liquids, namely, 1-ethyl-3-methylimidazolium iodide (EMII) + 1,3-dimethylimidazolium iodide (DMII) + 1-ethyl-3-methyl-imidazolium tetracyanoborate (EMITCB)[29,30] as one of the most promising and stable electrolyte components for a DSC with tungsten-based cathodes. The practical electrolyte for DSC was formulated by the addition of iodine, N-butylbenzoimidazole (NBB), and guanidinium thiocyanate (GNCS) in molar proportions 12:12:16:1.67:3.33:0.67 (EMII:DMII:EMITCB:I_2:NBB:GNCS);[29] this electrolyte is further coded Z952. To decrease the viscosity of Z952, various organic solvents (acetonitrile, sulfolane, methoxypropionitrile, propionitrile) were added, of which propionitrile (PN) turned out to be the best choice from the points of view of performance, volatility, and toxicity. The viscosity decrease is motivated by the assumption that the mass transport is Stokesian, that is, the molar conductivity is proportional to viscosity (Walden rule).[31] Although these solutions also show significant non-Stokesian (Grotthus-type) transport,[29,30,32,33] lowering of viscosity is still beneficial for enhancement of their conductivity.

To assess the diffusion of triiodide, I_3^- which is a key process controlling the electrolyte performance in DSC, so-called symmetrical dummy cells were used.[34,35] They were fabricated from two identical Pt−FTO electrodes with a thin layer of electrolyte solution sandwiched between them. Cyclic voltammogram (CV) of triiodide/iodide redox reaction

$$I_3^- + 2e^- \rightarrow 3I^- \tag{1}$$

in such a dummy cell gives rise to a plateau limiting current density, j_L, at sufficient overvoltages. It is controlled by the mass transport in the electrolyte solution

$$j_L = 2nFcD/\delta \tag{2}$$

where $n = 2$ is the number of electrons in reaction 1, F is the Faraday constant, c is the concentration of diffusion-limited species, D is the diffusion coefficient, and δ is the distance between electrodes in a dummy cell. The transport-controlling ion is I_3^- because its size is bigger and its concentration in Z952 ($c = 0.22$ M) is much smaller than that of I^- (3.18 M).

An alternative method for determining D is electrochemical impedance spectroscopy (EIS). The impedance spectrum of a dummy cell can be fitted to an equivalent circuit shown in Figure S1 (Supporting Information),[34] where R_S is the ohmic serial resistance, Z_W is the Nernst diffusion, and CPE is the

constant phase element describing deviation from the ideal capacitance, due to the electrode roughness. The low-frequency semicircle in the spectrum is diagnostic for mass transfer, expressed as Warburg impedance:

$$Z_W = \frac{W}{\sqrt{i\omega}}\tanh\sqrt{\frac{i\omega}{K_N}} \tag{3}$$

where W is the Warburg parameter and $K_N = (D/0.25\delta^2)$.[34−36] The high-frequency semicircle provides the values of R_s, R_{CT}, and Z_{CPE}. The latter element equals

$$Z_{CPE} = B(i\omega)^{-\beta} \tag{4}$$

where B and β are frequency-independent parameters of the CPE ($0 \leq \beta \leq 1$).

Figure S2 (Supporting Information) presents examples of electrochemical data for the pure ionic liquid Z952 in a model symmetrical dummy cell with two Pt−FTO electrodes. In addition, Figure S3 (Supporting Information) shows the corresponding data for the PN + Z952 mixtures. This initial screening of electrolytes was completed by their testing in solar cells with sensitized TiO_2 photoanodes and Pt−FTO cathodes at approximately 1 sun illumination. The data collected in Table S1 (Supporting Information) confirm that the solar conversion efficiency improves upon PN addition.

Figure 1 plots the diffusion coefficients, found independently by CV and EIS for all the electrolyte solutions tested. If the PN
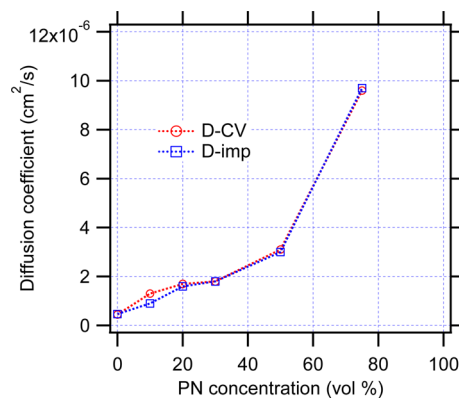
Figure 1. Diffusion coefficient of I_3^- in electrolyte solutions composed of Z952 ionic liquid with varying amount of added propionitrile (PN). Data from cyclic voltammetry (D-CV) and impedance spectroscopy (D-imp).

concentration equals zero, the coefficient approaches the literature value of 6×10^{-7} cm^2/s for a eutectic melt of ionic liquids, similar to Z952.[29] The addition of 50% (v/v) PN increases the diffusion coefficient 5 times to 3×10^{-6} cm^2/s. In all cases, there is good matching of the D values from CV and EIS, as previously reported by others.[32,37−39]

In practical DSCs, triiodide is produced by the dye regeneration occurring at the mesoporous photoanode, and I_3^- is subsequently transported to the cathode. Here, it should be reduced at a rate equal to or higher than the speed of I_3^- transport and dye regeneration. This quantifies the required exchange current density at cathode, j_0 to be comparable with photocurrent density on the TiO_2 photoanode. The latter is ca. 20 mA/cm^2 in good cells under AM 1.5 solar illumination.[3] The exchange current density equals

22344

dx.doi.org/10.1021/am506324d | ACS Appl. Mater. Interfaces 2014, 6, 22343−22350

$$ j_0 = \frac{RT}{nFR_{CT}} = Fk_0(c_{ox}^{1-\alpha} c_{red}^{\alpha}) \tag{5} $$

where R is the gas constant, T is temperature, R_{CT} is the charge-transfer resistance, k_0 is the formal (conditional) rate constant of the electrode reaction, c_{ox} and c_{red} are the concentrations of oxidized and reduced mediator, respectively, and α is the charge-transfer coefficient ($\alpha \approx 0.5$). For $j_0 = 20$ mA/cm^2, we calculate $R_{CT} = 1.3$ $\Omega\cdot$cm^2. Trancik et al.[40] proposed softer conditions for a cathode, which would, eventually, replace Pt–FTO in a dye-sensitized solar cell: R_{CT} of 2–3 $\Omega\cdot$cm^2, $T_{550} >$ 80%, and sheet resistance of 20 Ω/sq.

Fitting the EIS data in Figures S1 and S2 (Supporting Information) provides the following R_{CT} values for the Pt–FTO cathode (in $\Omega\cdot$cm^2): 0.36, 0.30, 0.18, 0.26, 0.13, and 0.55 for the electrolyte solutions of Z952 with 0, 10, 20, 30, 50, and 75% (v/v) of added propionitrile. Presumably, the highest R_{CT} for 75% addition of PN reflects the lowest concentrations of I$^-$ and I$_3^-$ on diluting the Z952 with PN. Although all the found values are better than required by eq 5, the optimum R_{CT} was attained for a solution with 50% PN. Hence, this medium was selected for all other studies reported below.

While the above-described evaluation routine of both mass transport and electrocatalytic activity is applicable for symmetrical dummy cells with two flat Pt–FTO electrodes, the corresponding electrodes from W/PEN grids present considerably more complicated geometry. Figure 2 shows the cross-
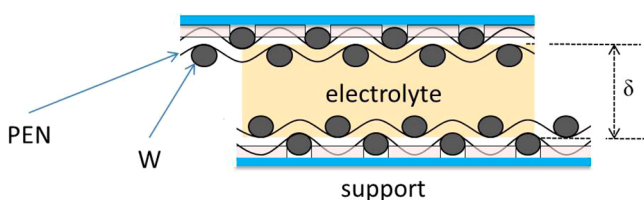
Figure 2. Scheme of a symmetrical dummy cell with electrodes fabricated from W/PEN grids. The Sefar A16 grid is woven from W-wires (20 μm in diameter) and PEN fiber (40 μm in diameter). The distance between adjacent W-wires is about 150 μm. The support is a PET foil, which is fixed by epoxy glue to the woven grid.

sectional scheme of such a symmetrical dummy cell. In this work, we used the Sefar A16 grid, which is characterized by small W-wire diameters (20 μm) and spacing (150 μm). The optical transmittance of the naked A16 grid is close to 90% over the whole visible spectrum, but it drops to ca. 80% for a practical electrode made by fixing of the A16 grid onto a PET-foil support by epoxy glue (Figure S4, Supporting Information). This optical transmittance is still near that of FTO glass (Figure S4, Supporting Information).

Figure 3a shows the texture of our A16 grid via scanning electron microscopy (SEM). The total area of W-wires in a 1 cm^2 area of the grid is 0.37 cm^2. The electrochemical deposition of Pt is documented in Figure 3c,d and referenced to a blank W-wire (Figure 3b). The tungsten metal is poor electrocatalyst for I$_3^-$/I$^-$, but it can be activated for application in DSC by thermal oxidization, forming a layer of substoichiometric surface oxide ($\approx$WO$_{2.6}$) at 500 °C in air.[41] However, this thermal treatment cannot be applied to our W/PEN grids. Hence, the grids need to be activated by a low-temperature platinization. SEM images show that Pt is deposited homogeneously over the whole surface of W-wire in the form of nanoparticles (ca. 50–200 nm in size) and in occasional

micron-size curved chips. A detailed image of Pt nanoparticles is shown in Figure S5 (Supporting Information).

If we assume 100% faradaic efficiency of electrodeposition, the actual current/time of electrolysis (4 mA/cm^2 and 45 s, respectively; see the Experimental Section) corresponds to ca. 90 μg/cm^2 of Pt, normalized to the grid area, or 240 μg/cm^2 normalized to the W-wires area. Similar Pt loading ($\approx$ 5–1000 μg/cm^2) was used by others for various preparations of DSC cathodes,[42−44] but the usual Pt@FTO cathodes made by pyrolysis of H$_2$PtCl$_6$ are at the lower limit (5–10 μg/cm^2) of this range. The thermally grown Pt nanoparticles are also smaller, ca. 5–20 nm.[43,44]

The Grid/Grid configuration shown in Figure 2 is characterized by a nonhomogeneous electrical field between the electrodes, and the distance δ is less accurately defined than in FTO/FTO cells due to deformations in the fabric and penetration of sealant into the grid. Figure 4 shows the cyclic voltammograms and impedance spectra at the Grid/Grid cell, referenced to a control device with two Pt–FTO electrodes, δ = 89 μm. The reference FTO/FTO cell was designed to have similar size as the Grid/Grid cell, including the dead spaces covered by the seal and contact edges ca. (2.5 × 2.5 cm^2) and comparable spacing δ. Considering the complications of the Grid/Grid cell, we can conclude that (1) The fitting of its EIS spectrum is less good particularly at low frequencies, which illustrates that the simple model equivalent circuit (Figure S1, Supporting Information) is now applicable only with limitations. (2) The mass transport of I$_3^-$ is roughly 2 times slower in the Grid/Grid configuration. (3) The grid is favored over FTO by considerably smaller ohmic serial resistance R_s (1.5 vs 8.2 $\Omega\cdot$cm^2) which obviously reflects the smaller sheet resistance of the grid.[26−28] (4) The charge transfer resistance R_{CT} of platinized W-grid is similar or even better than that of Pt–FTO. The found values are 0.59 $\Omega\cdot$cm^2 and 0.76 $\Omega\cdot$cm^2 for Pt–W and Pt–FTO, respectively, from the data in Figure 4 assuming the model in Figure S2 (Supporting Information) is applicable for the fitting of high-frequency part of impedance spectrum.

To bypass the inherent geometric limitations of the Grid/Grid dummy cell, we further investigated the behavior of an asymmetric dummy cell, in which one electrode is Pt–FTO and the second one is the Pt–W/PEN grid. Figure 5 shows the corresponding cyclic voltammogram and impedance spectrum. An obvious advantage of the asymmetric cell is that it avoids the uncertainty of spacing δ in all-grid cell (cf. Figure 2). More specifically, the effective value of δ can be now simply calculated from eq 2 using the known diffusion coefficient D of triiodide and the limiting current, j_L, controlled by the I$_3^-$ transport toward the FTO surface. It is measured when FTO is connected as the working electrode and biased negatively (Figure 5, left, line a). If we reverse the contacts, the corresponding mirror curve is obtained (Figure 5, left, line b). The asymmetric cell allows accurate comparison of the I$_3^-$ transport toward the flat surface of FTO and toward the complicated surface of W-wires in the fabric, independent of the geometry of the latter. Again, we note a factor of about 2 difference between both materials and a characteristic slow growth of j_L with overpotential, which will not be discussed here. Interestingly, the impedance spectrum is now fitted to the simple equivalent circuit (Figure S1, Supporting Information) with reasonable accuracy even for low frequencies (Figure 5 right).
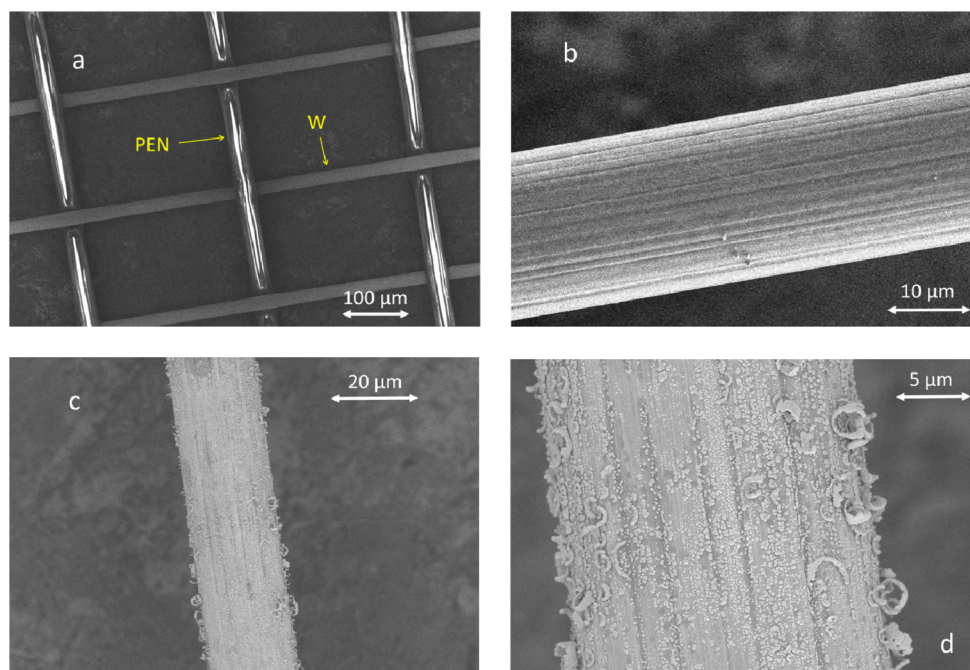
Figure 3. Scanning electron microscopy images of (a) A16 grid, (b) detail of a W-wire in the grid, and (c and d) the W-wire with electrodeposited Pt nanoparticles.
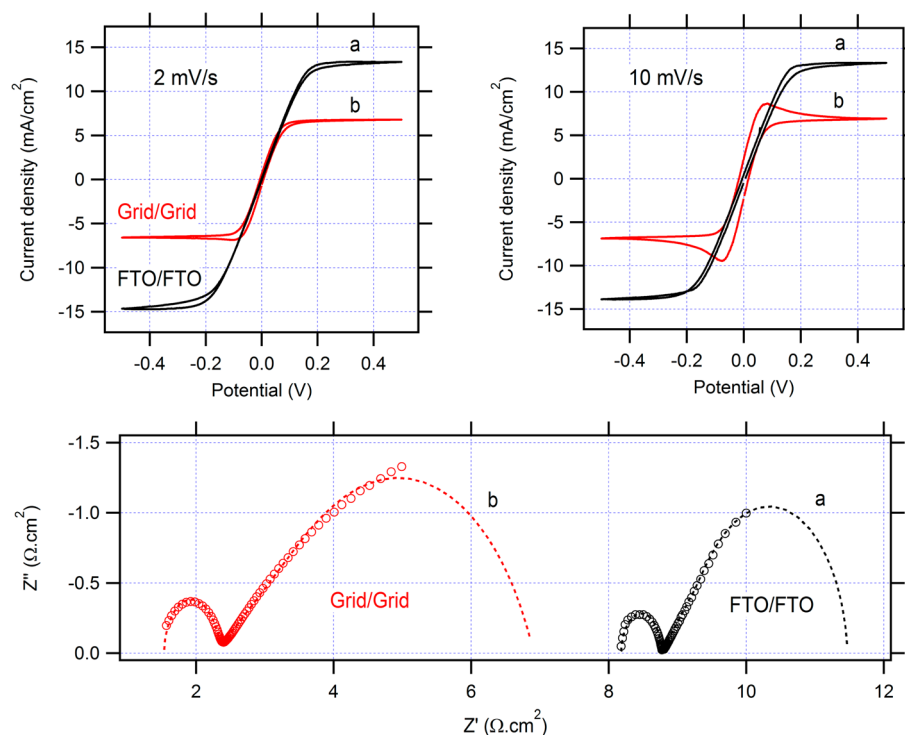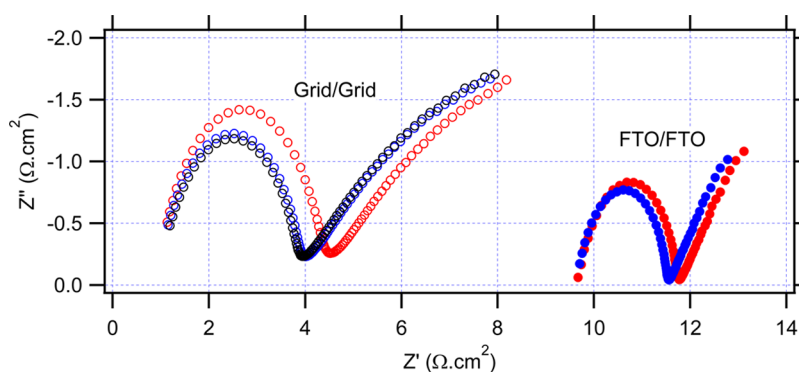

Figure 4. Elecrochemical data on symmetrical dummy cells with either (a) two platinized FTO electrodes (FTO/FTO) or (b) two platinized W-grids (Grid/Grid). The interelectrodes spacing (defined by the Surlyn foil seal) is 89 μm for the FTO/FTO cell. Electrolyte solution is composed of Z952 ionic liquid with 50 vol % propionitrile. (Top) Cyclic voltammetry, scan rate 2 or 10 mV/s, and (bottom) Nyquist plot of electrochemical impedance spectra measured at 0 V from 300 kHz to 0.1 Hz. Experimental data (red and black ○) were fitted to the equivalent circuits shown in Figure S2 (Supporting Information), and the fits are displayed as dashed lines.

Electrochemical stability of our Pt−W/PEN fabric electrode was tested by applying a bias of 0.5 V to the symmetrical dummy cell, which roughly corresponds to the maximum (diffusion-limited) current load to the cell. This test is actually more severe than requested for a proper function of illuminated DSC. The reason is that only cathodic current flows at the counterelectrode in the illuminated DSC at its operation. However, in the symmetrical dummy cell, both cathodic and anodic current load is applied on the tested electrodes. Figure 6 confirms excellent stability of our Pt−W/PEN grids against
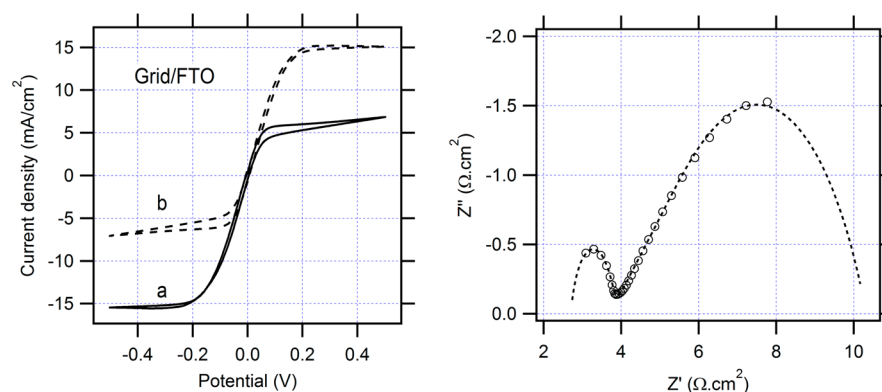
Figure 5. Elecrochemical data on nonsymmetrical dummy cells with one platinized FTO electrode and one platinized W-grid electrode (Grid/FTO). Electrolyte solution is composed of Z952 ionic liquid with 50 vol % propionitrile. (Left, a) Cyclic voltammetry, scan rate 5 mV/s, and (b) voltammogram on the same cell but with reversed contacts. (Right) Nyquist plot of electrochemical impedance spectra measured at 0 V from 300 kHz to 0.1 Hz. Experimental data (O) were fitted to the equivalent circuits shown in Figure S2 (Supporting Information), and the fit is displayed by dashed line.

Figure 6. Elecrochemical stability test on symmetrical dummy cells with either two platinized FTO electrodes (FTO/FTO; red, black, and blue O) or two platinized W-grids elecrodes (Grid/Grid; red and blue ●). Electrolyte solution is composed of Z952 ionic liquid with 50 vol % propionitrile. Nyquist plot of electrochemical impedance spectra measured at 0 V from 300 kHz to 0.1 Hz. (Red) Virgin cell, (black) cell after 15 min current load at 0.5 V bias, and (blue) cell after 15 h of current load at 0.5 V bias.

both cathodic and anodic breakdown in this test. There was no apparent deterioration of the electrodes, but even some small improvement of R_{CT} values, which is also observed in the FTO/FTO system, but it is not discussed here.

Yet another stability test was carried out by repeated measurements of electrochemical impedance after a certain time of aging at room temperature and open circuit. (Before each measurement of impedance spectrum, the dummy cell was subjected to one short voltammetric scan; see the Experimental Section). The top curve in Figure 7 shows impedance spectrum of a freshly assembled dummy cell, and each next curve toward bottom is the spectrum remeasured after some time of aging (specified in the figure caption). We do not observe any significant changes after about a month of storage; the found fluctuation in EIS shape are ascribed rather to experimental errors and, possibly, also to fluctuation of room temperature, as the temperature of the cell was not monitored during this test. The aging of DSC cathodes is quite often ignored in works dealing with optimization and screening of electrode materials (with few exceptions[36−38,45,46]). This aging, also termed "poisoning", of electrocatalyst does not seem to be detrimental for proper function of DSC. This documented by long-term stability of practical devices, leading to a hypothesis that the poisoning stops at some level of aging.[39]

Finally, we tested the performance of our grid-based counterelectrodes in a practical dye-sensitized solar cell. Figure

8 shows the corresponding current/voltage characteristics at 10 and 100% sun illumination. The devices with W/PEN-grid-based cathode and with the traditional FTO-based cathode behave similarly, which is further documented by the detailed DSC parameters collected in Table 1. Our data confirm that the platinized W/PEN grid is a promising alternative for Pt−FTO cathode. The grid is favored over FTO by better sheet resistance, better optical transparence, mechanical flexibility and the assumed cheaper price.

3. CONCLUSION

The addition of propionitrile to the electrolyte which is based on eutectic melt of ionic liquids (Z952) improves the transport of triiodide and the solar conversion efficiency of dye-sensitized solar cells.

The woven fabric consisting of transparent PEN fibers in warp and electrochemically platinized tungsten wires in weft is applicable as a flexible cathode in liquid-junction dye-sensitized solar cells with the I_3^-/I^- redox mediator. The electrode outperforms the thermally platinized FTO in serial ohmic resistance, R_s (1.5 vs 8.2 Ω·cm^2), charge-transfer resistance for triiodide reduction (0.59 Ω·cm^2 vs 0.76 Ω·cm^2) and offers comparable or better optical transparency in the visible and, particularly, in the near-IR spectral region (≈80%).

The Pt−W/PEN cathode exhibits good stability during electrochemical loading with the maximum (diffusion-limited)
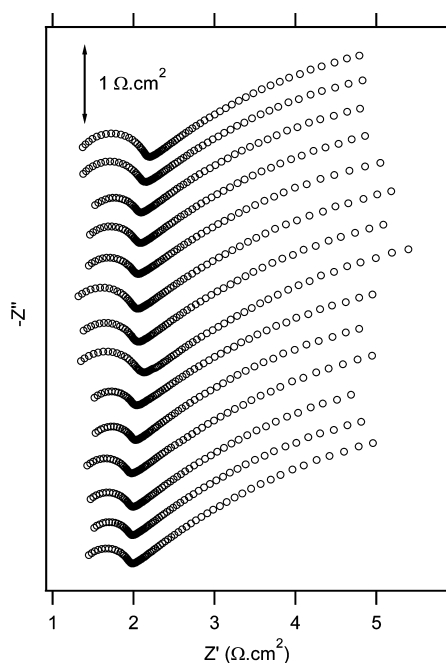
Figure 7. Long-term stability test by electrochemical impedance spectra on symmetrical dummy cell with two platinized W-grids elecrodes. The top curve is a Nyquist plot for a freshly assembled dummy cell. Each subsequent curve was measured after one or more days of aging; the actual aging time is (top to bottom) 0, 1, 2, 3, 4, 5, 6, 7, 8, 9, 10, 18, 19, 20, 26, and 27 days. Before each measurement, the cell was subjected to one cyclic voltammetry scan (from 0 V → 1 V → −1 V → 0 V, scan rate 50 mV/s) followed by 20 s relaxation at 0 V, followed by electrochemical impedance measurement at 0 V from 300 kHz to 0.1 Hz. Impedance spectra are offset in the $-Z''$ scale for better visualization.

current both in cathodic and anodic directions and during long-term (≈month) storage at open circuit.

The practical dye-sensitized solar cells with either Pt−W/PEN or Pt−FTO cathodes show similar performance, confirming that the former is a promising alternative for conductive glass in DSC counterelectrodes.

4. EXPERIMENTAL SECTION

4.1. Materials and Preparation of Electrodes. FTO glass was TEC 15 from Libbey-Owens-Ford, 15 Ω/sq. Platinized FTO (Pt−FTO) was prepared by depositing 5 μL/cm^2 of 10 mM H_2PtCl_6 in 2-propanol and calcination at 400 °C for 15 min. The symmetrical sandwich dummy cell was fabricated from two identical FTO sheets that were separated by Surlyn (DuPont) tape as a seal and spacer. The sheet edges of FTO were coated by ultrasonic soldering (Cerasolzer alloy 246, MBR Electronics GmbH) to improve electrical contacts. The distance between electrodes was measured by a digital micrometer. The cell was filled with an electrolyte through a hole in one FTO support which was finally closed by a Surlyn seal.

The woven fabric was obtained from Sefar (www.sefar.com). The Sefar A16 grid consists of transparent PEN fibers (diameter 40 μm) in warp and tungsten wires (diameter 20 μm) in weft. Spacing between PEN fibers is about 250 μm, and spacing between two W wires is about 150 μm. The W-wires were platinized by electrochemical deposition from 10 mM H_2PtCl_6 at 2.3 V for 45 s. The average current during electrodeposition was 4 mA/cm^2 (normalized to the total grid area). The dummy cell was assembled similarly to the FTO-based dummy cells but with te 3M End Seal (75 μm thickness) and Surlyn foils. Electrolyte was filled through two holes and channels in the seal. The edge contacts of grid-based electrodes were improved by silver paint.

Photoelectrochemical tests were carried out with TiO$_2$ films composed of 20 nm diameter anatase. The TiO$_2$ transparent films were deposited by screen printing onto fluorine-doped tin oxide (FTO, Solar 4 mm thickness, 10 ohms per square, Nippon Sheet Glass) conducting glass. Around 8 μm film was obtained by the number of screen-printing cycles and a ∼8 μm scattering layer (400 nm diameter, Catalysts & Chemicals Industries Co., Ltd. (CCIC), HPW-400) was deposited on the transparent layer. The TiO$_2$ electrode was sensitized with Na-cis-Ru^{II}(4,4′-bis(5-hexylthiophen-2-yl)-2,2′-bipyridine)(4-carboxylic acid-4′-carboxylate-2,2′-bipyridine)-(NCS)$_2$, which is coded C101. The DSC was assembled with a counter electrode using a Surlyn tape (25 μm in thickness) as a seal and spacer (see above). The cell active area for illumination was defined by a light-shading mask.

4.2. Methods. Electrochemical measurements were carried out using a PAR 273 potentiostat (EG&G) interfaced to a Solartron 1260A frequency response analyzer and controlled by a CorrWare program and Autolab PGstat-30 equipped with the FRA module (Ecochemie) controlled by the GPES-4 software. Electrochemical impedance data were processed using Zplot/Zview software. The impedance spectra were acquired in the frequency range from 300 kHz to 0.1 Hz, at 0 V bias voltage, the modulation amplitude was 10 mV. Before each measurement of impedance spectrum, the dummy cell was subjected to one fast voltammetric scan (between −1 and 1 V, 50 mV/s) followed by 20 s relaxation at 0 V. The optical spectra were measured by Varian Cary 5 spectrometer with integrating sphere in transmission mode. The reference spectrum was air. For photoelectrochemical tests, the light source was a 450 W xenon light source (Osram XBO 450, Germany) with a filter (Schott 113). The light power was regulated to the AM 1.5G solar standard by using a
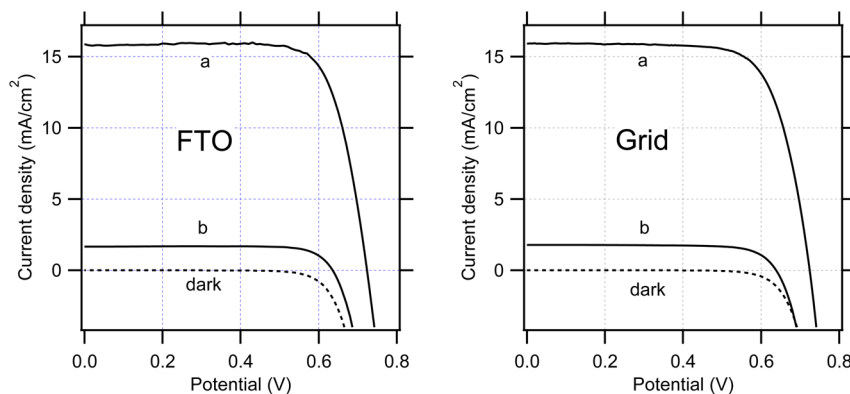
Figure 8. Current−voltage characteristics of (right) dye-sensitized solar cell with sensitized TiO$_2$ photoanode and platinized W/PEN-grid cathode and (left) a control device with Pt−FTO cathode. The illumination intensity is (a curves) 1 sun, (b curves) 0.1 sun, ("dark" curves) and 0.

Table 1. Characteristics of Solar Cells With C101-Sensitized TiO$_2$ Photoanodes at 1 and 0.1 Sun Illumination[a]

counterelectrode	illumination (sun)	j_{SC} (mA/cm^2)	V_{OC} (mV)	FF	η (%)
grid	0.1	1.79	638	0.75	8.5
grid	1	15.9	724	0.73	8.4
FTO	0.1	1.67	634	0.79	8.4
FTO	1	15.8	723	0.76	8.7

[a]Electrolyte solution is Z952 with 50% propionitrile. Short-circuit photocurrent density, j_{SC}; open-circuit voltage, V_{OC}; fill factor, FF; and solar conversion efficiency, η. The cell active area was 0.3 cm^2.

reference Si photodiode equipped with a color-matched filter (KG-3, Schott) to reduce the mismatch between the simulated light and AM 1.5G to less than 4% in the wavelength region of 350−750 nm. The differing intensities were regulated with neutral wire mesh attenuator. The applied potential and cell current were measured using a Keithley model 2400 digital source meter.

ASSOCIATED CONTENT

Ⓢ Supporting Information

Equivalent circuit for EIS fitting, additional electrochemical data on dummy cells, detailed results of solar cells tests, optical spectra, and high-resolution SEM image of Pt nanoparticles at W-wire. This material is available free of charge via the Internet at http://pubs.acs.org.

AUTHOR INFORMATION

Corresponding Author

*E-mail: kavan@jh-inst.cas.cz.

Notes

The authors declare no competing financial interest.

ACKNOWLEDGMENTS

REFERENCES

(1) Grätzel, M. Photoelectrochemical Cells. *Nature* **2001**, *414*, 338−344.

(2) O'Regan, B.; Grätzel, M. A Low-Cost High-Efficiency Solar Cell Based on Dye-Sensitized Titanium Dioxide. *Nature* **1991**, *353*, 737−740.

(3) Hagfeldt, A.; Boschloo, G.; Sun, L.; Kloo, L.; Pettersson, H. Dye-Sensitized Solar Cells. *Chem. Rev.* **2010**, *110*, 6595−6663.

(4) Grätzel, M. The Light and Shade of Perovskite Solar Cells. *Nat. Mater.* **2014**, *13*, 838−842.

(5) Zhou, H.; Chen, Q.; Li, G.; Luo, S.; Song, T. B.; Duan, H. S.; Hong, Z.; You, J.; Liu, Y.; Yang, Y. Interface Engineering of Highly Efficient Perovskite Solar Cells. *Science* **2014**, *345*, 542−546.

(6) Yun, H. G.; Kim, M.; Kang, M. G.; Lee, I. H. Cost-Effective Dye-Sensitized Solar Cells Consisting of Two Metal Foils Instead of Transparent Conductive Oxide Glass. *Phys. Chem. Chem. Phys.* **2012**, *14*, 6448−6451.

(7) Molla, M. Z.; Mizukoshi, N.; Furukawa, H.; Ogomi, Y.; Pandey, S. S.; Ma, T.; Hayase, S. Transparent Conductive Oxide-less Back Contact Dye-sensitized Solar Cells Using Cobalt Electrolyte. *Prog. Photovoltaics* **2014**, DOI: 10.1002/pip.2526.

(8) Fuke, N.; Fukui, A.; Komiya, R.; Islam, A.; Chiba, Y.; Yanagida, M.; Yamanaka, R.; Han, L. New Approach to Low-Cost Dye-Sensitized Solar Cells with Back Contact Electrodes. *Chem. Mater.* **2008**, *20*, 4974−4979.

(9) He, J.; Lee, L. T. L.; Yang, S.; Li, Q.; Xiao, X.; Chen, T. Printable Highly Catalytic Pt- and TCO-Free Counter Electrode for Dye-Sensitized Solar Cells. *ACS Appl. Mater. Interfaces* **2014**, *6*, 2224−2229.

(10) Xiao, Y.; Wu, J.; Yue, G.; Lin, J.; Huang, M.; Fan, L.; Lan, Z. The Surface Treatment of Ti Meshes for Use in Large-Area Flexible Dye-Sensitized Solar Cells. *J. Power Sources* **2012**, *208*, 197−202.

(11) He, W.; Qiu, J.; Zhuge, F.; Li, X.; Lee, J. H.; Kim, Y. D.; Kim, H. K.; Hwang, Y. H. Advantages of Using Ti-Mesh Type Electrodes for Flexible Dye-Sensitized Solar Cells. *Nanotechnology* **2012**, *23*, 225602.

(12) Cha, S. I.; Kim, Y.; Hwang, K. H.; Shin, Y. J.; Seo, S. H.; Lee, D. Y. Dye-sensitized Solar Cells on Glass Paper: TCO-Free Highly Bendable Dye-Sensitized Solar Cells Inspired by the Traditional Korean Door Structure. *Energy Environ. Sci.* **2012**, *5*, 6071−6075.

(13) Vijayakumar, V.; Du Pasquier, A.; Birnie, D. P., III Electrical and Optical Studies of Flexible Stainless Steel Mesh Electrodes for Dye Sensitized Solar Cells. *Sol. Energy Mater. Sol. Cells* **2011**, *95*, 2120−2125.

(14) Fan, X.; Wang, F.; Chu, Z.; Chen, L.; Zhang, C.; Zou, D. Conductive Mesh Based Flexible Dye-Sensitized Solar Cells. *Appl. Phys. Lett.* **2007**, *90*, 073501−0735013.

(15) Huang, W.; Zhang, X. L.; Huang, F.; Zhang, Z.; He, J.; Cheng, Y. B. An Alternative Flexible Electrode for Dye-Sensitized Solar Cells. *J. Nanopart. Res.* **2012**, *14*, 838.

(16) Murakami, T. N.; Grätzel, M. Counter Electrodes for DSC: Application of Functional Materials as Catalysts. *Inorg. Chim. Acta* **2008**, *361*, 572−580.

(17) Tathavadekar, M.; Biswal, M.; Agarkar, S.; Giribabu, L.; Ogale, S. Electronically and Catalytically Functional Carbon Cloth as a Permeable and Flexible Counter Electrode for Dye Sensitized Solar Cell. *Electrochim. Acta* **2014**, *123*, 248−253.

(18) Sun, J.; Li, Y.; Peng, Q.; Hou, S.; Zou, D.; Shang, Y.; Li, Y.; Li, P.; Du, Q.; Wang, Z.; Xia, Y.; Xia, L.; Li, X.; Cao, A. Macroscopic, Flexible, High-Performance Graphene Ribbons. *ACS Nano* **2013**, *7*, 10225−10232.

(19) Akbar, Z. A.; Lee, J. S.; Kang, J.; Joh, H. I.; Lee, S.; Jang, S. Y. FTO-Free Counter Electrodes for Dye-Sensitized Solar Sells Using Carbon Nanosheets Synthesised from a Polymeric Carbon Source. *Phys. Chem. Chem. Phys.* **2014**, *16*, 17595−17602.

(20) Bao, Z.; Xie, H.; Rao, J.; Chen, L.; Wei, Y.; Li, H.; Zhou, X. High Performance of Pt/TiO$_2$-Nanotubes/Ti Mesh Electrode and Its Application in Flexible Dye-Sensitized Solar Cell. *Mater. Lett.* **2014**, *124*, 158−160.

(21) Toivola, M.; Halme, J.; Miettunen, K.; Aitola, K.; Lund, P. D. Nanostructured Sye Solar Cells on Flexible Substrates-Review. *Int. J. Energy Res.* **2009**, *33*, 1145−1160.

(22) Kim, J.; Kang, J.; Jeong, U.; Kim, H.; Lee, H. Catalytic, Conductive, and Transparent Platinum Nanofiber Webs for FTO-Free Dye-Sensitized Solar Cells. *ACS Appl. Mater. Interfaces* **2013**, *5*, 3176−3181.

(23) Kim, H.; Veerappan, G.; Park, J. H. Conducting Polymer Coated Non-Woven Graphite Fiber Film for Dye-sensitized Solar Cells: Superior Pt- and FTO-Free Counter Electrodes. *Electrochim. Acta* **2014**, *137*, 164−168.

(24) Xu, J.; Li, M.; Wu, L.; Sun, Y.; Zhu, L.; Gu, S.; Liu, L.; Bai, Z.; Fang, D.; Xu, W. A Flexible Polypyrrole-Coated Fabric Counter

22349

dx.doi.org/10.1021/am506324d | *ACS Appl. Mater. Interfaces* 2014, 6, 22343−22350

Electrode for Dye-Sensitized Solar Cells. *J. Power Sources* **2014**, *257*, 230−236.

(25) Yun, M. J.; Cha, S. I.; Seo, S. H.; Lee, D. Y. Highly Flexible Dye-Sensitized Solar Cells Produced by Sewing Textile Electrodes on Cloth. *Sci. Rep.* **2014**, *4*, 5332−53326.

(26) Kylberg, W.; De Castro, F. A.; Chabrecek, P.; Geiger, T.; Heier, J.; Nicholson, P. G.; Nueesch, F.; Theocharous, E.; Sonderegger, U.; Hany, R. Spatially Resolved Photocurrent Mapping of Efficient Organic Solar Cells Fabricated on a Woven Mesh Electrode. *Prog. Photovoltaics* **2013**, *21*, 652−657.

(27) Kylberg, W.; De Castro, F. A.; Chabrecek, P.; Sonderegger, U.; Chu, B. T. T.; Nueesch, F.; Hany, R. Woven Electrodes for Flexible Organic Photovoltaic Cells. *Adv. Mater.* **2011**, *23*, 1015−1019.

(28) Castro, F. A.; Chabrecek, P.; Hany, R.; Nueesch, F. Transparent, Flexible, and Low-Resistive Precision Fabric Electrode for Organic Solar Cells. *Phys. Status Solidi RRL* **2009**, *3*, 278−280.

(29) Bai, Y.; Cao, Y.; Zhang, J.; Wang, M.; Li, R.; Wang, P.; Zakeeruddin, S. M.; Grätzel, M. High-Performance Dye-Sensitized Solar Cells Based on Solvent-Free Electrolytes Produced from Eutectic Melts. *Nat. Mater.* **2008**, *7*, 626−630.

(30) Zakeeruddin, S. M.; Grätzel, M. Solvent-Free Ionic liquid Electrolytes for Mesoscopic Dye-Sensitized Solar Cells. *Adv. Funct. Mater.* **2009**, *19*, 2187−2202.

(31) Bentley, C. L.; Bond, A. M.; Hollenkamp, A. F.; Mahon, P. J.; Zhang, J. Concentration and Electrode Material Dependence of the Voltammetric Response of Iodide on Platinum, Glassy Carbon and Boron-Doped Diamond in the Room Temperature Ionic Liquid 1-Ethyl-3-methylimidazolium Bis(trifluoromethanesulfonyl)imide. *Electrochim. Acta* **2013**, *109*, 554−561.

(32) Zistler, M.; Wachter, P.; Wasserscheid, P.; Gerhard, D.; Hinsch, A.; Sastrawan, R.; Gores, H. J. Comparison of Electrochemical Methods for Triiodide Diffusion Coefficient Measurements and Observation of Non-Stokesian Diffusion Behaviour in Binary Mixtures of Two Ionic Liquids. *Electrochim. Acta* **2006**, *52*, 161−169.

(33) Zistler, M.; Wachter, P.; Schreiner, C.; Gores, H. J. Electrochemical Measurement of Triiodide Diffusion Coefficients in Blends of Ionic Liquids: Results for Improving a Critical Parameter of Dye-Sensitized Solar Cells. *J. Mol. Liq.* **2010**, *156*, 52−57.

(34) Kavan, L.; Yum, J.-H.; Grätzel, M. Graphene Based Cathodes for Liquid-Junction Dye Sensitized Solar Cells: Electrocatalytic and Mass Transport Effects. *Electrochim. Acta* **2014**, *128*, 349−359.

(35) Fabregat-Santiago, F.; Bisquert, J.; Palomares, E.; Otero, L.; Kuang, D.; Zakeeruddin, S. M.; Grätzel, M. Correlation between Photovoltaic Performance and Impedance Spectroscopy of Dye-Sensitized Solar Cells Based on Ionic Liquids. *J. Phys. Chem. B* **2007**, *111*, 6550−6560.

(36) Hauch, A.; Georg, A. Diffusion in the Electrolyte and Charge-Transfer Reaction at the Platinum Electrode in Dye Sensitized Solar Cells. *Electrochim. Acta* **2001**, *46*, 3457−3466.

(37) Kavan, L.; Yum, J.-H.; Nazeeruddin, M. K.; Grätzel, M. Graphene Nanoplatelet Cathode for Co(III/II) Mediated Dye-Sensitized Solar Cells. *ACS Nano* **2011**, *5*, 9171−9178.

(38) Kavan, L.; Yum, J.-H.; Grätzel, M. Graphene Nanoplatelets Outperforming Platinum as the Electrocatalyst in Co-Bipyridine Mediated Dye-Sensitized Solar Cells. *Nano Lett.* **2011**, *11*, 5501−5506.

(39) Kavan, L.; Yum, J.-H.; Grätzel, M. Optically Transparent Cathode for Co(II/III) Mediated Dye-Sensitized Solar Cells Based on Graphene Oxide. *ACS Appl. Mater. Interfaces* **2012**, *4*, 6999−7006.

(40) Trancik, J. E.; Barton, S. C.; Hone, J. Transparent and Catalytic Carbon Nanotube Films. *Nano Lett.* **2008**, *8*, 982−987.

(41) Uppachai, P.; Harnchana, V.; Pimanpang, S.; Amornkitbamrung, V.; Brown, A. P.; Brydson, R. M. D. A Substoichiometric Tungsten Oxide Catalyst Provides a Sustainable and Efficient Counter Electrode for Dye-sensitized Solar Cells. *Electrochim. Acta* **2014**, *145*, 27−33.

(42) Chen, C. M.; Chen, C. H.; Wei, T. C. Chemical Deposition of Platinum on Metallic Sheets as Counterelectrodes for Dye-Sensitized Solar Cells. *Electrochim. Acta* **2010**, *55*, 1687−1695.

(43) Papageorgiou, N.; Maier, W. E.; Grätzel, M. An Iodide/Triiodide Reduction Electrocatalyst for Aqueous and Organic Media. *J. Electrochem. Soc.* **1997**, *144*, 876−884.

(44) Papageorgiou, N. Counter-Electrode Function in Nanocrystal-line Photoelectrochemical Cell Configurations. *Coord. Chem. Rev.* **2004**, *248*, 1421−1446.

(45) Kavan, L.; Yum, J.-H.; Grätzel, M. Optically Transparent Cathode for Dye-Sensitized Solar Cells Based on Graphene Nano-platelets. *ACS Nano* **2011**, *5*, 165−172.

(46) Wu, M.; Lin, X.; Wang, L.; Guo, W.; Qi, D.; Peng, X.; Hagfeldt, A.; Grätzel, M.; Ma, T. Economical Pt-Free Catalysts for Counter Electrodes of Dye Sensitized Solar Cells. *J. Am. Chem. Soc.* **2012**, *134*, 3419−3428.